



Measurements of morphodynamics of a sheltered beach along the Dutch Wadden Sea

Marlies A. van der Lugt^{1, 2}, Jorn W. Bosma³, Matthieu A. de Schipper¹, Timothy D. Price³, Marcel C.G. van Maarseveen³, Pieter van der Gaag¹, B. Gerben Ruessink³, Ad J.H.M. Reniers¹, and Stefan G.J. Aarninkhof¹

¹Delft University of Technology, Delft, The Netherlands

²Deltares, Delft, The Netherlands

³Utrecht University, Utrecht, The Netherlands

Correspondence: Marlies van der Lugt (m.a.vanderlugt@tudelft.nl)

Abstract. A field campaign was carried out at a sheltered sandy beach with the aim of gaining new insights into the driving processes behind sheltered beach morphodynamics. Detailed measurements of the local hydrodynamics, bed level changes and sediment composition were collected at the man-made beach on the leeside of the barrier island Texel, bordering the Marsdiep basin that is part of the Dutch Wadden Sea. The data set consists of (1) current, wave and turbidity measurements from a dense cross-shore array and a 3 km alongshore array, (2) sediment composition data from beach surface samples, (3) high-temporal-resolution RTK-GNSS beach profile measurements, (4) a pre-campaign spatially covering bathy-topo map and (5) meteorological data. This manuscript outlines how these measurements were set up and how the data have been processed, stored and can be accessed. The novelty of this data set lies in the detailed approach to resolve forcing conditions on a sheltered beach, where sediment transport is governed by a strong interplay between tidal currents, waves and bed composition, primarily due to the low-energy (near-threshold) forcing. The data is publicly available at 4TU Centre for Research Data at DOI: 10.4121/19c5676c-9cea-49d0-b7a3-7c627e436541.v1 (van der Lugt et al., 2023).

1 Introduction

Sheltered coastlines are traditionally defended by hard coastal structures made of concrete, asphalt or stones. Recently, projects using an alternative method have been proposed, where flood defences have been reinforced with sandy foreshores to upgrade them in anticipation of sea level rise (Perk et al., 2019; Ton et al., 2021). Although the use of sand has been postulated to be a sustainable approach to coastal maintenance of wave-dominated coasts (Stive et al., 2013; Grunnet et al., 2005; Brand et al., 2022), sandy reinforcements in low-energy environments (Jackson et al., 2002; Vila-Concejo et al., 2010; Ton, 2023) are not as established. This partly explains why well-documented field observations at these sites are scarce.

The morphodynamic evolution of sandy beaches in sheltered environments is governed by both waves and currents (Freire et al., 2009). The wave forcing is generally characterised as low-energy: average fair weather wave heights are small ($H_{m0} < \mathcal{O}(0.25)$ m), and storms with onshore wind have maximum wave heights constrained by the geometry of the adjacent (semi-) enclosed basin ($H_{m0} < \mathcal{O}(1.5)$ m). The beach face often is narrow ($< \mathcal{O}(20)$ m) and morphological features are generally



inherited from storm events (Jackson et al., 2002; Nordstrom and Jackson, 2012). Even though beaches in estuaries and on the lee-side of islands are not truly fetch-limited, as refracting ocean swell waves may still reach the shore under the right
25 circumstances, they generally do classify as low-energy too (Cooper et al., 2007).

Previous studies have classified types and behavior of sheltered beaches based on the following indicators: the beach profile in terms of curvature, slope and presence of low-tidal terraces (Hegge et al., 1996; Eliot et al., 2006; Pickrill, 1985; Travers, 2007; Travers et al., 2010; Makaske and Augustinus, 1998), or more traditionally in terms of Dean number (Wright and Short, 1984). However, these classifications co-exist as no single-one is able to describe the rich variety of beach states found in
30 sheltered environments. Besides, such classifications also do not help predict upcoming morphodynamic changes or the effects of maintenance and/or nourishment strategies, as they generally describe naturally occurring beaches with an equilibrium profile.

In addition, sheltered beaches are often limited in extent, both in the nourished as well as in the natural setting. Consequently, alongshore gradients and large-scale circulation patterns or residual currents are drivers of typical morphological features
35 of sheltered areas, such as shoals and spits (Hopkins et al., 2017; Van Kouwen et al., 2023). Therefore, a process-based understanding of beach development of sheltered beaches is believed to be the way forward, such that the balance between local geometry, sediment type and forcing can be resolved explicitly.

Detailed hydrodynamic studies of sheltered beaches are scarce (Vila-Concejo et al., 2010), but are needed as it is not evident that the skill of engineering morphodynamic models, which have been tried-and-tested on exposed coasts (e.g., Huisman et al., 2019; Luijendijk et al., 2017; Hegermiller et al., 2022; Splinter and Palmsten, 2012), directly translate to low-energy
40 environments too. This is particularly the case for the unresolved and therefore parameterized transport processes that are calibrated on field and lab observations.

First of all, in low-energy environments, tidal and wind-driven currents are expected to play a relatively larger role in sediment mobility and profile shape compared to beaches in wave-dominated environments (Bernabeu et al., 2003; Jackson and Nordstrom, 1992; Nordstrom and Jackson, 2012; Colosimo et al., 2023). For example, tidal currents enhance wave-induced bed-shear stresses (Kleinhans and Grasmeijer, 2006) and may simultaneously alter the dominant transport direction from cross-shore to alongshore (Héquette et al., 2008).

Second, the sea state itself is expected to differ between sheltered and open coasts. At sheltered sites, the wave state is generally locally generated. Young sea state wave spectra are more isotropic than their deep-water counterparts and are therefore
50 expected to have a wider directional spreading as well as a more gradual decay of energy with frequency (Donelan et al., 1985; Young et al., 1996; Ewans, 1998) compared to fully developed sea states. Additionally, the wave direction is modulated by the tide through the interaction of waves with the tidal current (Hopkins et al., 2016). These processes affect the strength and direction of wave radiation stresses, and thus the extent to which the wave field drives alongshore currents that could transport sediment (Feddersen, 2004).

Third, the restorative capacity of wave-driven onshore transport by returning sediment high in the beach profile from lower parts after storm erosion (Hoefel and Elgar (2003)) is limited on low-energy beaches (Hegge et al., 1996; Jackson et al., 2002; Nordstrom and Jackson, 2012). The active part of the profile at a given moment, i.e., the part of the cross-section in which



60 sediment is moved up and down by waves, is smaller on low-energy beaches (Hallermeier, 1980; Ton et al., 2021), meaning that the tide will play a larger role in vertically displacing the sediment (Valiente et al., 2019), corresponding to larger relative tidal ranges (Masselink and Short, 1993).

Finally, the nourished sediment composition does not always match the natural gradation. Sediment heterogeneity, although widely recognized as an important control in beach development (e.g., Huisman et al., 2016; Bergillos et al., 2018), is generally inadequately accounted for or resolved in sediment transport models. Hiding and exposure of grains with widely varying diameters due to the way they are vertically sorted significantly complicates the response of the bed to hydrodynamic forcing (Kleinhans, 2005; McCarron et al., 2019), as the entrainment threshold of the different grains can be highly modified (e.g., Choule J. Sonu, 1972; Guillén and Hoekstra, 1996; Masselink et al., 2010; Richmond and Sallenger, 1985). Especially on low-energy beaches, which are often supply-limited, mixed sediments with a distinctive coarse fraction forming an armor/wear layer (Strypsteen et al., 2021) are an appealing option to limit erosion. Yet, how the local grain-size distribution and its spatial heterogeneity resulting from the implemented sediment mixture affects sediment pathways at a mixed-energy site requires more field data before transport models can be improved accordingly.

The extent to which these aforementioned processes are resolved in the transport equations of engineering-type models requires validation. Therefore, there is a need for detailed intra-wave information on the vertical velocity profile, as well as the grainsize sorting and wave shape on top of bulk statistics such as mean water levels, and significant wave heights and periods.

We capitalize on the realization of a sheltered sandy foreshore bordering the Dutch Wadden Sea by collecting high-resolution (in space and time) data on hydrodynamic forcing, bed composition and bathymetric changes shortly after construction. This paper presents data of a 6 week campaign (referred to as SEDMEX) as well as background data of bed levels and sediment composition data in the 2 years prior. This campaign was not the first to investigate fetch-limited hydrodynamics, sheltered-beach morphodynamics or mixed-sediment dispersal, but it is one of the first campaigns to combine all these different types of observations of an entirely man-made beach. Through this measuring campaign, we aim to add to the already extensive data set of exposed coastal nourishments (e.g., Huisman et al., 2019; de Schipper et al., 2016; Ludka et al., 2018; Lemke and Miller, 2017; Soulsby, 1999; Kroon et al., 1995; Guillén and Hoekstra, 1996). This data set can then help to further expand the types of environments for which tried-and-tested process-based models of nourishment lifetime and development exist. The overall aim of this study is to unravel the drivers of mixed-sediment transport in a low-energy system and to be able to validate model parameterization of unresolved processes (e.g., wave non-linearity, wave breaking, multi-fraction sand transport) in engineering-type models at sheltered beaches. This data set is made available for use by the broader coastal research and engineering community as a benchmark test case for process-based models of sheltered systems with complex sediment mixtures.

2 Field site Prins Hendrik Zanddijk, the Netherlands

The campaign was undertaken at the Prins Hendrik Zanddijk (PHZD), a sandy coastal defense along the Wadden Sea coast of the island Texel constructed in 2019 (Figure 1a). The Wadden Sea near Texel is connected to open sea through the tidal inlet



Marsdiep. The Marsdiep branches into several channels, of which the basin's main channel Texelstroom flows parallel to the field site. Tides in the basin are semi-diurnal with MHW=NAP+0.6 m and MLW=NAP-0.7 m. NAP is the local Dutch datum, roughly equal to mean sea level. The vertical tidal range varies from 1 to 2 m between neap and spring tide. Tidal velocities in the Texelstroom along the PHZD reach up to 1 m/s and can increase further under influence of local winds. The majority of waves approaching the PHZD here are short-crested ($T < 5$ s), locally generated within the basin over a fetch of 5-25 km
95 depending on the wind direction. However, under specific conditions, swell waves from the SSW propagate into the basin through the Marsdiep and can refract towards the coastline too, but with diminishing amplitude. Under these circumstances small infragravity waves can reach the shore ($H_{m0,ig} \sim 0.15$ m observed).

The South-East section of the islands' coastline used to be protected by an asphalt-covered dike of approximately 3 km
100 (Figure 1b, annotated as 'Dike'). In 2019 it was upgraded with a sandy reinforcement consisting of an 8 m high dune parallel to the old dike and an attached 3 m high sand spit that created a shallow lagoon behind the dike and the spit, enabling the seaward discharge from an existing water pumping station meanwhile providing habitat for foraging birds (Figure 1b and Perk et al. (2019)). This sandy foreshore was designed to withstand normative storm conditions of a storm with return period of 4000 years. The nourishment is constructed on top of the existing sub-tidal flat Schanserwaard, over which the tidal currents in
105 the deep (up to 25 meter depth) tidal channel Texelstroom are slowed down. The composition of the bed of the Schanserwaard is mixed: both sand and silt are found. The core of the nourishment was constructed with fine sand ($d_{50} 200 \mu\text{m}$), similar to the native sand. A 0.5-1 m thick top-layer of coarser sand ($d_{50} > 400 \mu\text{m}$) along the water line reduces sediment mobility. The sub-aerial section of the spit is additionally armoured with a top layer of shells to reduce aeolian transport (Perk et al., 2019; Strypsteen et al., 2021).

110 All measurements in this campaign were collected near the water line at the seaward side of the nourishment.

3 SEDMEX campaign

The field campaign was undertaken during the autumn of 2021 between September-09 and October-19. The measurements consisted of an array of instruments to capture the cross-shore wave and current transformation, and an alongshore array of wave and current observations to investigate alongshore variability in hydrodynamics. Wave height and periods were recorded
115 from pressure recording instruments. Directional wave parameters and near bed orbital and mean velocities were computed from velocity recording instruments. For their locations see Figure 2. Starting September-25, these wave observations were augmented with wave observations in the tidal channel Texelstroom (at 20 m water depth). Here, a Xylem Motus heave-pitch-roll wave buoy was deployed, measuring at 4 Hz.

3.1 Hydrodynamic instrument deployments

120 On the spit beach, the wave transformation over the subtidal flat towards the beach was monitored over a cross-shore array. Along the nourishment, the alongshore variability was monitored with a series of instruments at constant water depth.

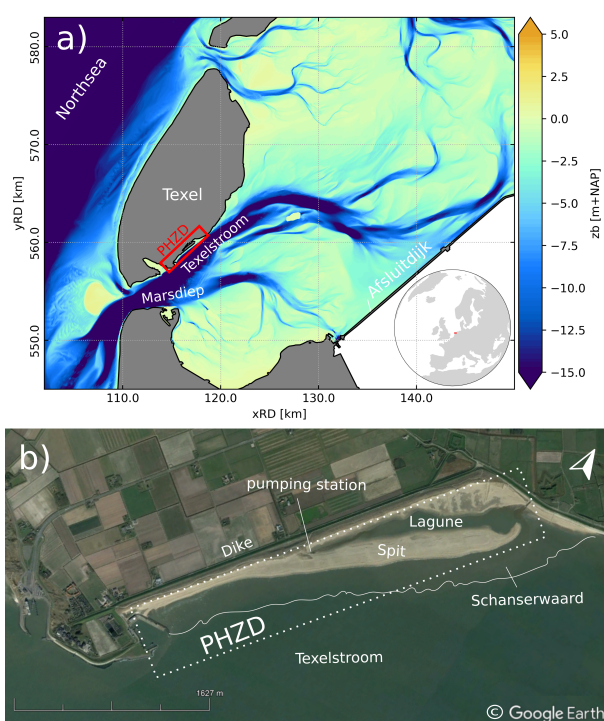


Figure 1. a) Location of the PHZD on the south-east side of the Dutch island Texel along the Wadden Sea. Colors indicate the bed elevation in m NAP with NAP being the local datum at approximately mean sea level, b) Aerial image of the field site. Sandy parts visible in the dotted rectangle are the sub-aerial parts of the PHZD nourishment.

The instrument set-up of the cross-shore array (Figure 3), focuses on high-frequency observations of near-bed orbital velocity, pressure and currents to be able to study intra-wave processes. All instruments were mounted to poles jettied into the bed and/or frames attached to the poles. The array consisted of 7 Acoustic Doppler Velocimeters (ADV's). Of those, 4 were Nortek
125 Vectors, sampling velocity at 16 Hz, 15 cm above the bed. Three of these ADV's were installed with additional RBRsolo³ pressure sensor measuring at 8 Hz, also positioned 15 cm above the bed to obtain pressure measurements at equal height above the bed as velocity measurements. Three vertically stacked Sontek ADV's were positioned centrally in the array at NAP-0.85 m, measuring at 10 Hz. Three Ocean Sensor Systems OSSI pressure sensors spaced equidistantly between the most offshore ADV and the nearshore array were deployed at 15 cm above the bed measuring at 10 Hz. A downward looking Nortek Acoustic
130 Doppler Current Profiler (ADCP) was placed in front of the beach face at NAP-1.2 m, measuring at 4 Hz in 50 mm bins in 1800 s burst mode. The location on the cross-shore profile and the instrument's configuration are summarized in Table 1. Throughout the experiment, bed levels at the instrument locations varied for instruments close to the water line. The instrument heights were adjusted several times throughout the campaign to match the target height above bed after morphodynamic changes. The horizontal x,y-position of the instruments was not changed.

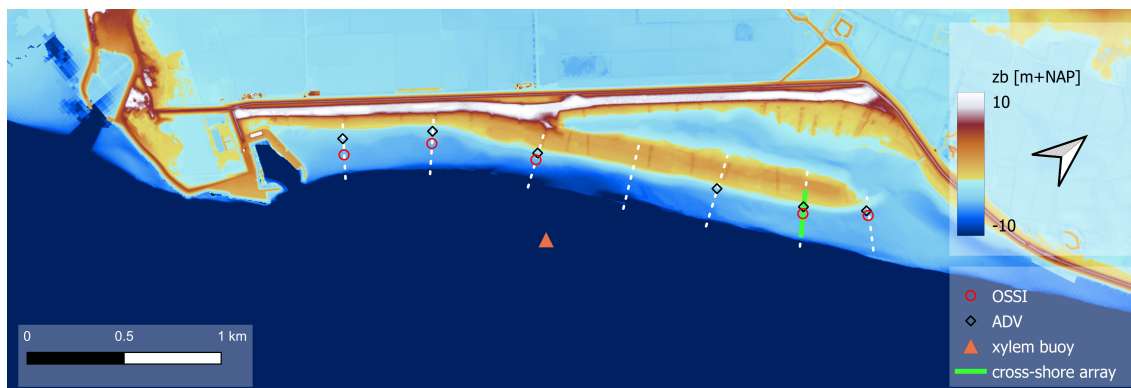


Figure 2. Nearshore bathymetry and topography with location of alongshore instruments, reference position of monitored cross-shore transects (dashed-white) and location of the cross-shore array (solid-green).

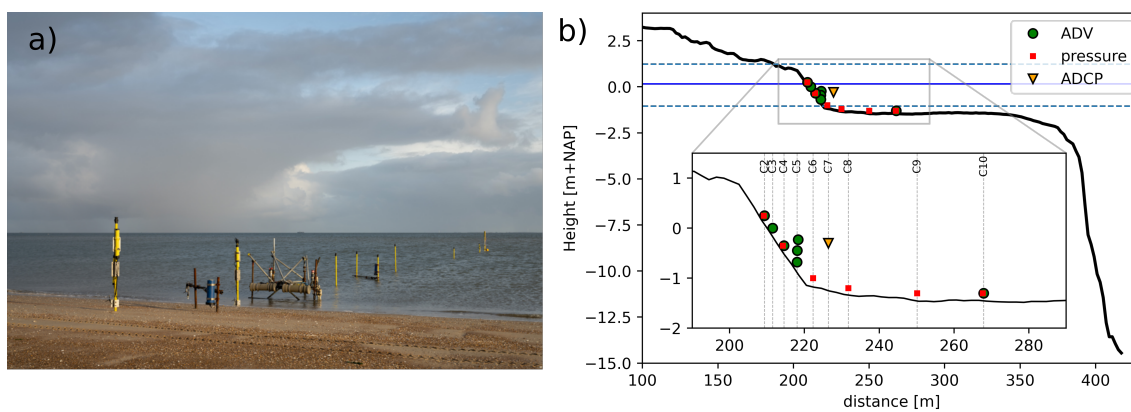


Figure 3. a) Impression of the cross-shore instruments and their mounts. b) Location of the instruments on the cross-shore array. Bathymetry at the beginning of the campaign in solid black lines, mean recorded water level in solid blue and maximum and minimum recorded water levels during SEDMEX campaign in dashed blue.

135 Alongshore, 6 Nortek Vector ADV's at NAP-0.75 m and 5 OSSI pressure sensors at NAP-1.45 m were deployed that allow
 for studying alongshore variability in presence of North Sea swell, residual flow and local windsea. Figure 2 shows their
 position along the PHZD. Similar to the instruments in the cross-shore array, the instrument heights were adjusted throughout
 the campaign to match the target height above bed.

140 A series of Seapoint Turbidity Meters (STMs) and Campbell OBS-3+ turbidity meters were co-located and synchronised
 with a selection of the current meters (ADV's and ADCP) to collect proxy data on suspended sediment concentration at 15 cm
 above the bed (Table 1).



Table 1. Configurations of the deployed hydrodynamic instruments

Instrument	Brand	Sampled quantity	Sampling frequency (Hz)	Height above bed (cm)	Initial bed level [m+NAP]	Configuration	Recording setting
L2C2SOLO	RBR Solo ³	pressure	8	15	0.1		continuous
L2C2VEC	Nortek Vector	velocity	16	15	0.1	sideways looking	30min bursts 10s I.O.
L2C3VEC	Nortek Vector	velocity	16	15	-0.15	downward looking	30min bursts 10s I.O.
L2C4SOLO	RBR Solo ³	pressure	8	15	-0.5		continuous
L2C4VEC		velocity	16	15	-0.5	sideways looking	30min bursts 10s I.O.
L2C5SONTEK3	SONTEK	velocity	10	65	-0.88	downward looking	30min bursts 60s I.O.
L2C5SONTEK2	SONTEK	velocity	10	40	-0.85	downward looking	30min bursts 60s I.O.
L2C5SONTEK1	SONTEK	velocity	10	15	-0.83	downward looking	30min bursts 60s I.O.
L6C1VEC	Nortek Vector STM	velocity turbidity	16	15	-0.80	downward looking	30min bursts 10s I.O.
L5C1VEC	Nortek Vector STM	velocity turbidity	16	15	-0.80	downward looking	30min bursts 10s I.O.
L4C1VEC	Nortek Vector OBS-3+	velocity turbidity	16	15	-0.85	downward looking	30min bursts 10s I.O.
L3C1VEC	Nortek Vector STM	velocity turbidity	16	15	-0.80	downward looking	30min bursts. 10s I.O.
L1C1VEC	Nortek Vector STM	velocity turbidity	16	15	-0.80	downward looking	30min bursts 10s I.O.
L4C1SOLO	RBR Solo ³	pressure	8	15	-0.85		continuous
L2C6OSSI	OSSI	pressure	10	15	-1.15		continuous
L6C2OSSI	OSSI	pressure	10	24	-1.45		continuous
L5C2OSSI	OSSI	pressure	10	24	-1.45		continuous
L4C3OSSI	OSSI	pressure	10	24	-1.45		continuous
L1C2OSSI	OSSI	pressure	10	24	-1.5		continuous
L2C7ADCP	Nortek Aquadopp STM	velocity profile turbidity	4	95	-1.2	downward looking	30min bursts 10s I.O.
L2C8OSSI	OSSI	pressure	10	15	-1.35		continuous
L2C9OSSI	OSSI	pressure	10	15	-1.45		continuous
L2C10SOLO	RBR Solo ³	pressure	8	15	-1.45		continuous
L2C10VEC	Nortek Vector	velocity	16	15	-1.45	downward looking	30min bursts 10s I.O.



4 Beach profile measurements

At the position of the instruments, beach profiles were collected on a bi-daily basis during low water with RTK-GNSS on top of a walking wheel to obtain continuous surveys from the dune, throughout the surf zone to approximately 1 m water depth. Each survey with the RTK-GNSS covered 7 target transects, see Figure 2. The bed level changes along these transects are part of a longer-term measurement series. All site visits spanning the period between 2019 and 2022 are available in the published data set.

To project the 1 Hz walking-wheel measurements to the same grid, each sample was allocated to its closest target transect coordinate, where the target transect was discretized with 0.25 m resolution. In case a sample was distanced more than 20 m from the target transect, it was discarded. Then, the bed level at the target coordinates was set to the average of all allocated GNSS-samples in the 0.25 m cross-shore section. In case no samples were assigned to the target coordinate, the bed level was set to NaN (Not a Number). NaNs are present in the data set for some dates and tracks at deeper coordinates, when set-up of the water level prohibited us from going any deeper into the water with the GNSS device. Additionally, there are a few NaNs in the data set due to occasionally walking faster than the 0.25 m cross-shore resolution divided by the sampling frequency.

5 Sediment sampling

Statistics on surface sediment samples together with RTK-GNSS location data are available for the PHZD intertidal beach. This includes compositional data of sediment samples collected along multiple cross-shore transects across the intertidal beach during the entire monitoring period (Figure 5a), and samples taken repeatedly at the same locations throughout multiple tidal cycles along one cross-shore transect (L2) during the SEDMEX period (Figure 5b). Additionally, a series of individual samples were taken at specific locations of interest such as the distal end of the spit.

Collection proceeded by inserting a small (6 cm high) empty jar upside down into the sand while rotating horizontally in an alternately (counter-)clockwise fashion (Figure 4a). Once filled up to a point where there was only about 1 cm left unfilled at the bottom of the jar, the jar was carefully turned upright whilst pulled out of the sand. An empty hand was used to quickly close off the opening to prevent any material from falling out in the process. The collected material was then siphoned into a pre-labeled plastic bag. However, on two days (at spring tide and neap tide), a sand-scraper device was alternatively used instead of a jar to obtain thin-layer samples (mm-scale) from the top 5 cm of the bed, which is in accordance with the sampling depth when using the jar. For more specifications of this device and details of the associated procedure the reader is referred to Van IJzendoorn et al. (2023). In all cases the filled sample bags were subsequently taken to a laboratory where their contents were oven-dried, mechanically sieved and weighed.

Drying of the sediment samples was achieved in one of two ways: (1) sub-samples of ~150 g were collected inside aluminium cups, after which they were dried mostly overnight at a temperature of 105° C, or (2) the opened plastic sample bags were put in the oven in their entirety at a lower temperature of 65° C for a duration of at least 4 days (Figure 4b-d). Once completely dry, ~150 g sub-samples were then emptied on top of a sieve tower standing on the platform of a mechanical shaker (Figure 4e).



Figure 4. Sediment-analysis procedure: (a) sample with a small glass jar, (b) collect material in plastic bag, (c) collect sub-sample inside aluminium cup, (d) dry sub-samples in oven, (e) shake sub-sample in sieve tower and (f) weigh each sieve with retained material.

175 The sieve shaker was turned on for approximately 15 minutes, after which the sieve tower was carefully removed from the platform. Each sieve was then weighed individually on an accurate semi-analytical balance. Measured weights were automatically inserted into a spreadsheet next to their previously measured empty weights. Snapshots of the entire procedure are presented in Figure 4.

180 Shells or their fragments were not removed from the mixture beforehand, so the analysed samples are composed of both biogenic and non-biogenic minerals. The generally flatter-shaped shell particles tend to end up in a sieve with an aperture close to the size of their second longest dimension, which is often substantially longer than their nominal length (i.e., as if they were spherical). As the mineral density of many calcium-carbonate shell types is similar to that of quartz sand (i.e., ~ 2650 g/L), this could result in an inaccurate size-by-weight distribution of the whole sample. However, in the samples, the non-biogenic sand fractions were much more abundant. Therefore, it is assumed that the effect of the biogenic material on the sediment-sample statistics is limited.

185 Mass data on the size fractions of the sediment samples were further processed using the open-access software GRADISTAT (Blott and Pye, 2001), to obtain grain-size distributions as well as a commonly reported statistics such as grain-size percentiles and standard deviations. All samples collected spanning the period between 2019 and 2022 are made available in the published

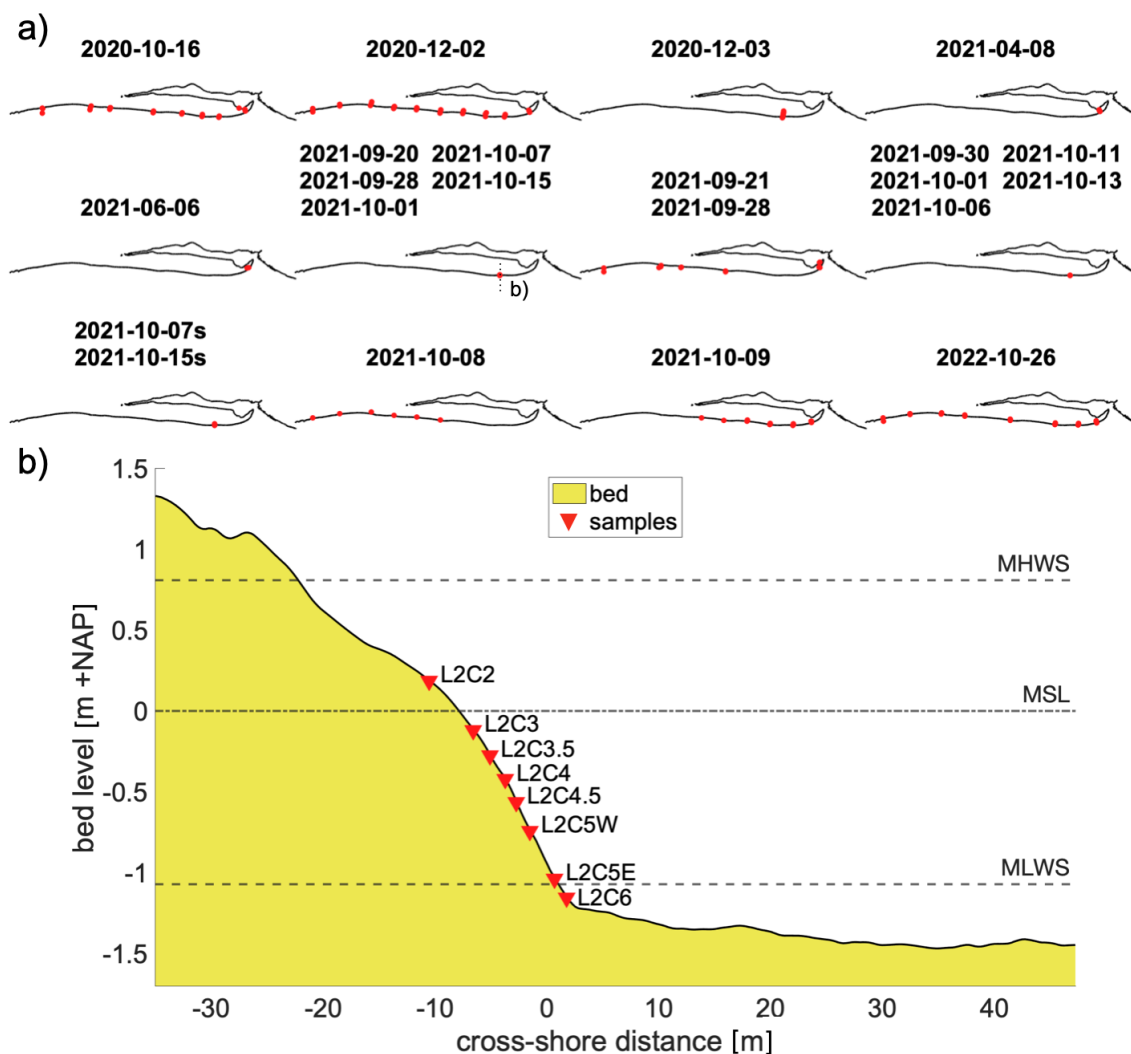


Figure 5. a) Overview of the horizontal locations of all sediment samples taken during the monitoring period. Multiple dates per subplot indicates samples were repeatedly taken on the exact same locations. On the two dates ending in an 's' the sand-scraper method was used. b) Vertical positions of the periodically collected samples along the L2 cross-shore instrument array. Horizontal dashed lines indicate the mean high water spring level (MHWS), mean sea level (MSL) and mean low water spring level (MLWS), respectively.

data set. In addition to the cumulative percentile values, the following statistics on the grain-size distributions are presented:
 190 mean (M_G), sorting (σ_G), skewness (Sk_G) and kurtosis (K_G). These are computed following Blott and Pye (2001) based on
 the geometric (modified) graphical measures of Folk and Ward (1957).



6 Hydrodynamic data processing

The presented hydrodynamic dataset consists of three folders: (1) raw data as recorded by the instruments, converted to a standardised data format in netCDF including all meta-data required for further interpretation, (2) quality checked (QC) data, where all continuous measurements are cut into blocks of 10 (ADV, pressure) or 30 (ADCP) minutes. For each block, outliers were identified and samples deemed too noisy were masked with a separate protocol for each instrument type as further discussed below. In case the signal contained sufficient valid samples ($< 5\%$ masked), the masked samples were replaced with cubic interpolation of the time-series, (3) tailored data, with burst-averaged wave and current characteristics, presented as a time series of statistics on a 10/30 minute resolution. All published data is recorded and saved in Central European Summer Time (GMT+2). The remainder of this section outlines the undertaken processing steps for each instrument group on top of the process described above.

6.1 Pressure

Pressure was recorded at the stand-alone pressure sensors, as well as the ADV's and ADCP. The recorded total pressure signals were corrected for air pressure fluctuations recorded on the dry beach. In the QC dataset, moments in time where the instrument fell dry were removed. Near-bed pressure was converted to surface elevation signals including a correction for depth attenuation using linear wave theory. The tailored dataset includes the following statistics: Significant wave height $H_{m0} = 4\sqrt{m_0}$, a few mean wave periods: $T_{m-1,0} = \frac{m-1}{m_0}$, $T_{m0,1} = \frac{m_0}{m_1}$, $T_{m0,2} = \sqrt{\frac{m_0}{m_2}}$ with m_n is the spectral moment of order n , the wave peak period and the smoothed wave peak period. All of these are computed in 10 minute blocks using linear wave theory in the frequency band [0.05-1.0] Hz. The smoothed peak period is the maximum of a parabolic fitting through the highest bin and two bins on either side the highest one of the discrete wave spectrum. Furthermore, wave non-linearity parameters skewness and asymmetry were included and computed from the near-bed pressure as:

$$Sk = \frac{\langle p^3 \rangle}{\langle p^2 \rangle^{\frac{3}{2}}} \quad (1)$$

$$As = \frac{\langle \mathcal{H}\{p\}^3 \rangle}{\langle p^2 \rangle^{\frac{3}{2}}} \quad (2)$$

with p the near-bed pressure signal in a frequency band that scaled with the peak period: $[0.5f_p - 2f_p]$ Hz, $\mathcal{H}p$ the Hilbert transformed pressure and $\langle \rangle$ representing averaging over the 10 min block.

6.2 ADV and ADCP

All ADVs and the ADCP recorded velocities in probe-coordinates XYZ, and the probe orientation of each instrument was measured in the field. In the QC dataset all velocity measurements were rotated to East-North-Up coordinates and samples were flagged as outlier based on 3 conditions: (1) too low instantaneous inter-beam correlation, (2) exceeding the instantaneous recordable velocity threshold (varying between 1.5-2.1 ms^{-1} for horizontal velocities dependent on horizontal or vertical placement of the instrument probe and 0.6 ms^{-1} for vertical velocities), (3) statistical outlier detection: if the recording was



more than 3 standard deviations from a block's mean it was flagged as outlier. Additionally, blocks were masked where the probe was less than 10 cm submerged based on the block's mean water depth. The correlation threshold was initially based on the criterion proposed by Elgar et al. (2005).

$$225 \quad c_{min} = (0.3 + 0.4 \cdot \sqrt{(s_f/25)}) \cdot 100 \quad (3)$$

with s_f the instrument's sampling frequency. This criterion rejected several blocks of which the block-averaged wave characteristics were well in line with the time series. Therefore, the QC data set is published with a lowered inter-beam correlation criterion of ($> 50\%$), to arrive at a more complete time series of block-averaged wave and flow characteristics in the tailored data set. The tailored data set further includes orbital velocities in frequency band $[0.5f_p - 4]$ Hz, mean wave direction θ_{mean} computed through linear wave theory and the method of maximum entropy (Lygre and Krogstadt, 1986), the component of the velocity signal in direction of wave propagation u_d and non-linearity parameters for the near-bed orbital velocity in the direction of wave propagation and pressure in the frequency band $[0.5f_p - 2f_p]$ Hz. The computation of non-linearity in the orbital velocities follows Equations 1-2 but with the velocity in the direction of wave propagation u_d instead of p . For the ADCP, these wave statistics were computed from the velocities recorded in the cell 15 cm above the bed and additionally, block-averaged velocity profiles and depth averaged velocities were recorded on the tailored data set.

Should a user want to apply a stricter correlation criterion to study for example turbulence, they can use the QC data set as starting point and proceed from there.

Calibration of the turbidity signal to in-situ collected sand samples was performed in the lab but suspended sediment concentrations (SSC) were difficult to relate to local hydrodynamics, most likely due to presence of mud in the basin (Pearson et al., 2021) and bubbles under breaking waves (Puleo et al., 2006). Therefore, the published QC dataset presents the unconverted turbidity signal, and SSC is not presented in the tailored dataset.

6.3 Overview quality checked hydrodynamic data

Figure 6 shows an overview of valid data bursts for all hydrodynamic instruments in the presented data set. Missing data is caused by various reasons. The first, planned cause of missing data is that some of the instruments were placed at positions that fell dry during part of the tidal cycle. Therefore, all instruments placed higher in the profile than NAP-0.80m delivered intermittent time series, with water levels governing the gaps. Moreover, several instruments were removed and re-installed twice during the campaign for a cleaning of the probe, a battery pack change and data retrieval. This leads to data gaps throughout the night of September-20 and the night of October-04. The RBR pressure logger L2C2SOLO was not redeployed on October-05. The Sontek ADV's ran on a single battery pack, which ran out of capacity around October-12.

Between September-28 and October-07, the beach profile at the cross-shore array underwent large changes and several instruments got buried, after which they were excavated and reinstalled, and got buried again. This has consequences for the data availability of L2C5SONTEK1, L2C4VEC, L2C4SOLO, L2C3VEC, L2C2VEC and L2C2SOLO.

Two instruments malfunctioned because of damage to the mounting material. Vector L3C1 was noticed to be rotated in its clamp on October-10, only possible after impact by a hard (floating) object. Analyses of the recorded velocities and directions



255 revealed this must have happened on October-03. Therefore, the data between October-03 and October-10 were removed from the data set. Similarly, the ADCP mounting frame was used by ignorant bypassing boaters as a mooring spot on October-09, which pulled the jetpoles skewed. The mounting poles were set straight again on October-10, intermediate data was discarded.

260 Lastly, some of the correlation and amplitude dropouts are believed to be caused by barnacle growth on transducer surfaces and/or seaweed getting stuck between legs of the probe. We visited the beach every other day and removed both barnacles and seaweed when identified, but had no control over what passed by in the intermediate times. We have relied on the quality control routine to remove bursts that suffer from seaweed, barnacles, or disturbance of the signal by cleaning the probe surfaces.

7 Environmental conditions

265 Figure 7 shows the wind speed and direction, water level, as well as significant wave height, mean period and near-bed velocities as measured on the deepest ADV (L2C10VEC) for the complete SEDMEX measuring campaign. The campaign captured two spring-neap tidal cycles, which allows for investigation of interaction between tides, wind-driven currents and wave-driven processes. Wind data is available from the nearest KNMI station De Kooy (10 km southward). The mean tidal range during the campaign was 1.25 m and varied between 0.5-1.8 m. The water level anomaly, estimated with a Godin filter of two times 24 hours and 1 of 25 hours, was positive for most of the campaign. Negative anomalies only occurred when the wind direction was Southwest to Northwest. The recordings started during a fair weather period starting September-10 to September-18. 270 The most energetic event occurred in the week September-30 to October-05, when strong winds caused ~30 cm setup (Figure 7b) in the tidal basin and south-southwesterly waves penetrated through the tidal inlet, partially refracting over the platform edge to the beach. On October-01, strong winds led to flow reversal over the entire platform, with flood-directed currents prevailing for three high tides (Figure 7c). A second period of very calm conditions started October-07 and lasted up to October-12.

275 In the offshore Texelstroom channel, significant wave heights reached up to 1 m, with corresponding peak period between 4-5 s (not plotted). Because of the platform depth of approximately NAP-1.4 m, waves of these heights broke on the platform edge. ADV L2C10VEC at NAP-1.45 m showed maximum wave height of 60 cm and peak wave periods of 3-3.5 s, indicating that not all wave energy in the channel reaches the beach (Figure 7d). Mean wave period on the platform generally relates with wind direction: onshore-directed winds generate wind waves in the basin with short-crested, short-period waves. With shore-parallel winds from the south-west, the peak period increases due to the longer fetch length of waves that penetrate the 280 tidal inlet from the North Sea (Figure 7e). 10 Minute time-averaged near-bed velocities on the platform directly seaward of the beach face are predominantly alongshore directed (Figure 7c).

8 Data samples

8.1 Cross-shore wave transformation

285 The cross-shore wave transformation governs where to expect wave-driven sediment transport and also determines whether this transport is onshore, offshore or alongshore directed. Figure 8 shows a snapshot of the recorded hydrodynamics on September-

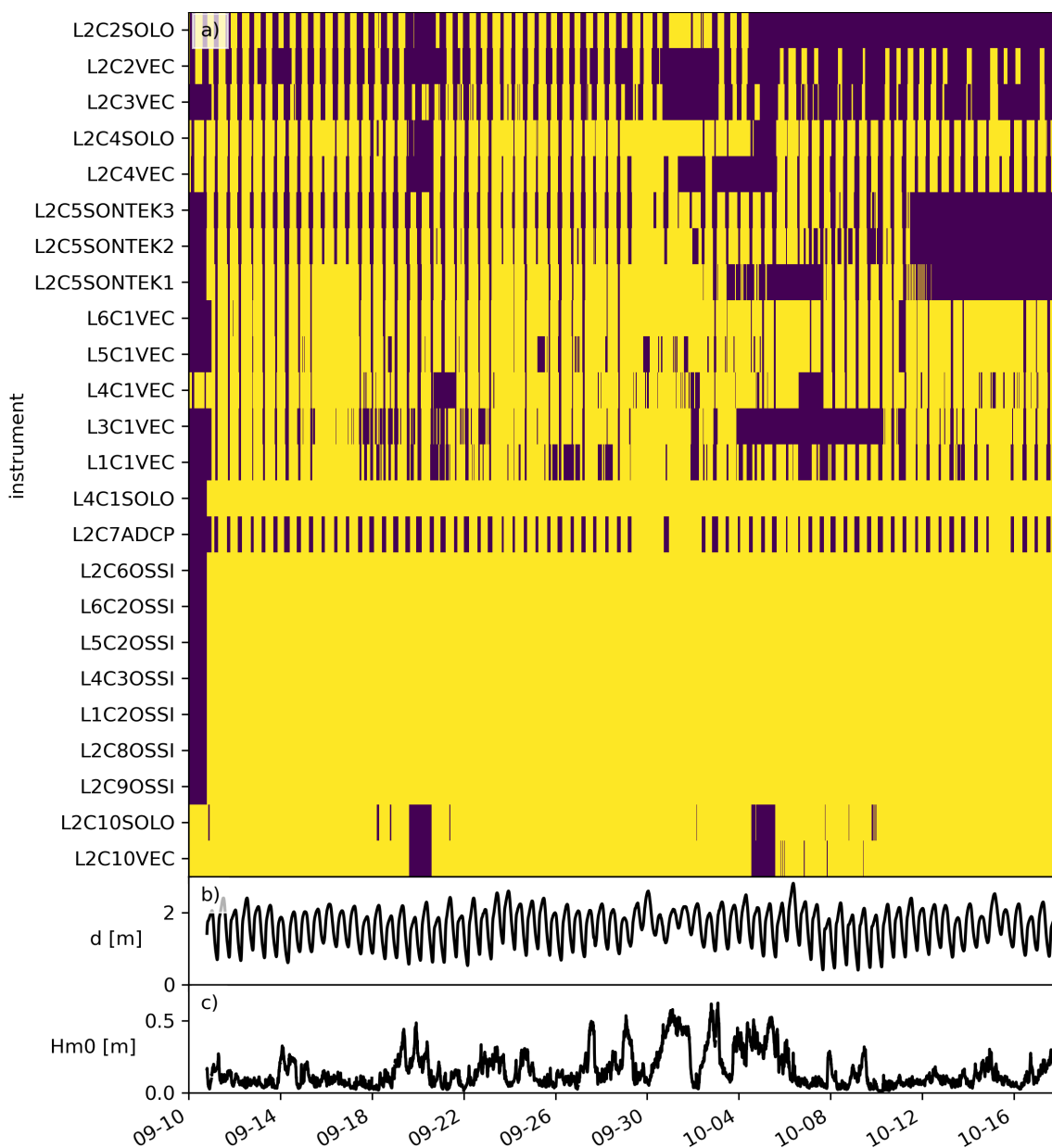


Figure 6. (a). Time series of available bursts of observations that passed the quality requirements, stacked per instrument. Yellow = available. Panels below show observations of (b) water level and (c) significant wave height at L2C9OSSI For reference.

19 at 08:30. Waves of 40 cm height propagated over the platform (Figure 8a), shoaled on the beach step and broke at water depths of ~ 1 m (Figure 8a). The waves were 20° oblique on the platform and turned shore normal over the beach face (Figure 8c). Wave skewness develops over the last 20 m towards the water line (Figure 8d). Near-bed orbital velocities increases

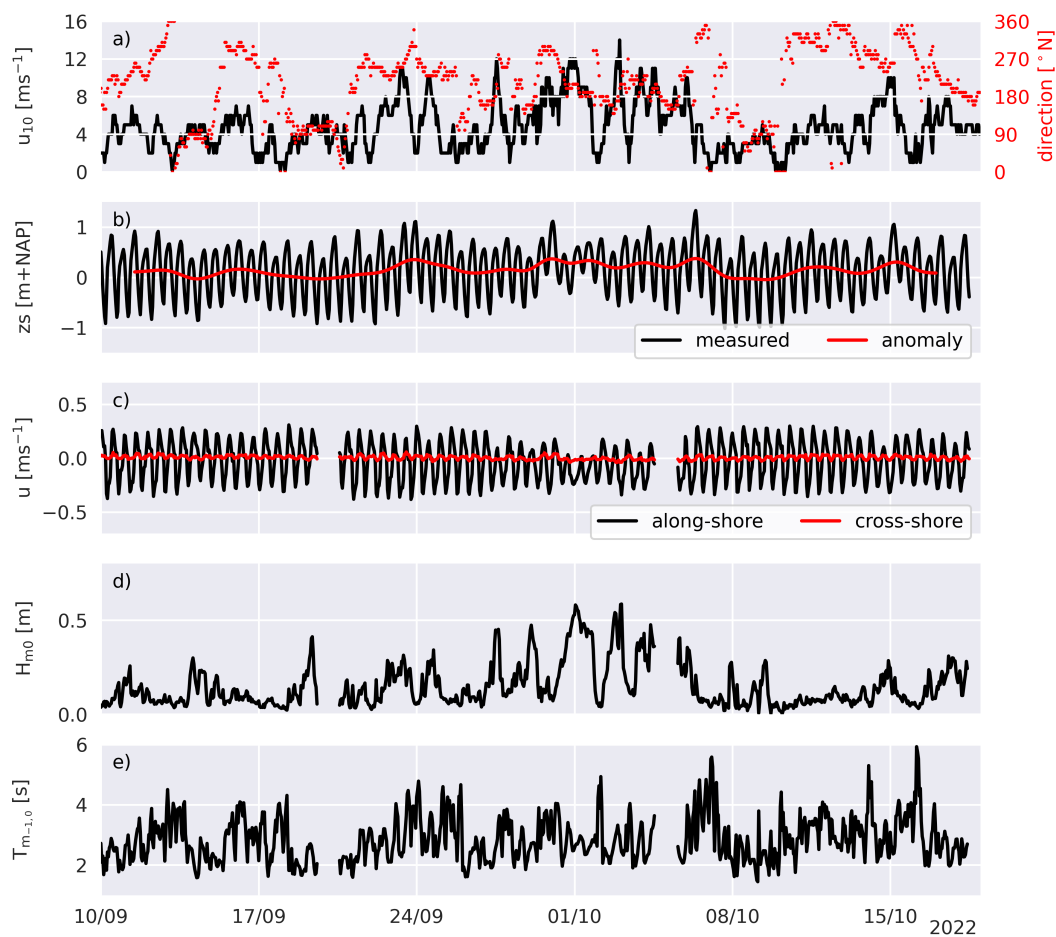


Figure 7. Hydrometeo conditions during the campaign: (a) wind speed and direction, (b) water level and water level anomaly, (c) alongshore and cross-shore flow velocity, (d) significant wave height at the deepest ADV on the platform and (e) mean wave period $T_{m-1,0}$ at that same ADV. The two data gaps are related to maintenance days.



over the beach face (Figure 8e), and near-bed cross-shore velocities near the waterline are offshore directed. Alongshore
290 (tidal) velocities first decrease with water depth, but then the wave-driven alongshore component increases the total alongshore
velocity again in even shallower water (Figure 8f).

8.2 Bed level changes

The cross-shore bed level was monitored throughout the SEDMEX campaign. During calm conditions with waves smaller than
30 cm, bed levels were stable. Significant bed level changes were recorded the first week of October 9. Several energetic days
295 caused continuous profile adjustments. Those adjustments are captured in the data set for six cross-sections along the entire
beach with approximately two-day temporal resolution.

8.3 Grain-size distributions

Surface sediments at the PHZD were found to be moderately to extremely poorly sorted, the latter often clearly visible from
the often polymodal grain-size distributions. An example of a relatively well-sorted distribution is shown in Figure 10. Never-
300 theless, the width of the distribution indicates the presence of a wide range of grain-size fractions.

9 Conclusions

A comprehensive data set of sheltered-beach hydrodynamic forcing and beach response has been presented of the 6-week field
campaign. The SEDMEX campaign was conducted on the Prins Hendrik Zanddijk, a sheltered man-made beach situated on the
lee side of the barrier island Texel in the Marsdiep basin of the Dutch Wadden Sea. This data set allows in-depth analysis of the
305 driving mechanisms of mixed-sediment transport at sheltered beaches in a process-based approach. In particular the interplay
between waves and currents and their effect on the beach face development. The duration of the campaign was sufficiently
long to capture a wide range of environmental conditions, giving insight into the (relative) importance of bed-shear stresses
induced by wind, waves and tides. Furthermore, sediment sorting processes can be studied based on the combination of sed-
iment samples and detailed hydrodynamic measurements. Additionally, we envision this data set will support the validation
310 of morphodynamic models (e.g. Delft3D, XBeach) on sheltered beaches. The high-temporal resolution observations addition-
ally allow for testing of intra-wave scale models in complex real-world applications. Altogether, this comprehensive data set
provides new data to improve our predictive understanding of morphodynamics in sheltered (semi-enclosed) systems, where
sediment transport is governed by a subtle interplay between waves, tidal currents and bed composition due to low-energy
(near-threshold) forcing.

315 10 Data availability

The data set presented in this article has been published at 4TU Centre for Research Data (van der Lugt et al., 2023) at DOI:
10.4121/19c5676c-9cea-49d0-b7a3-7c627e436541.v1 following the FAIR principles (Wilkinson et al., 2016). The hydrody-

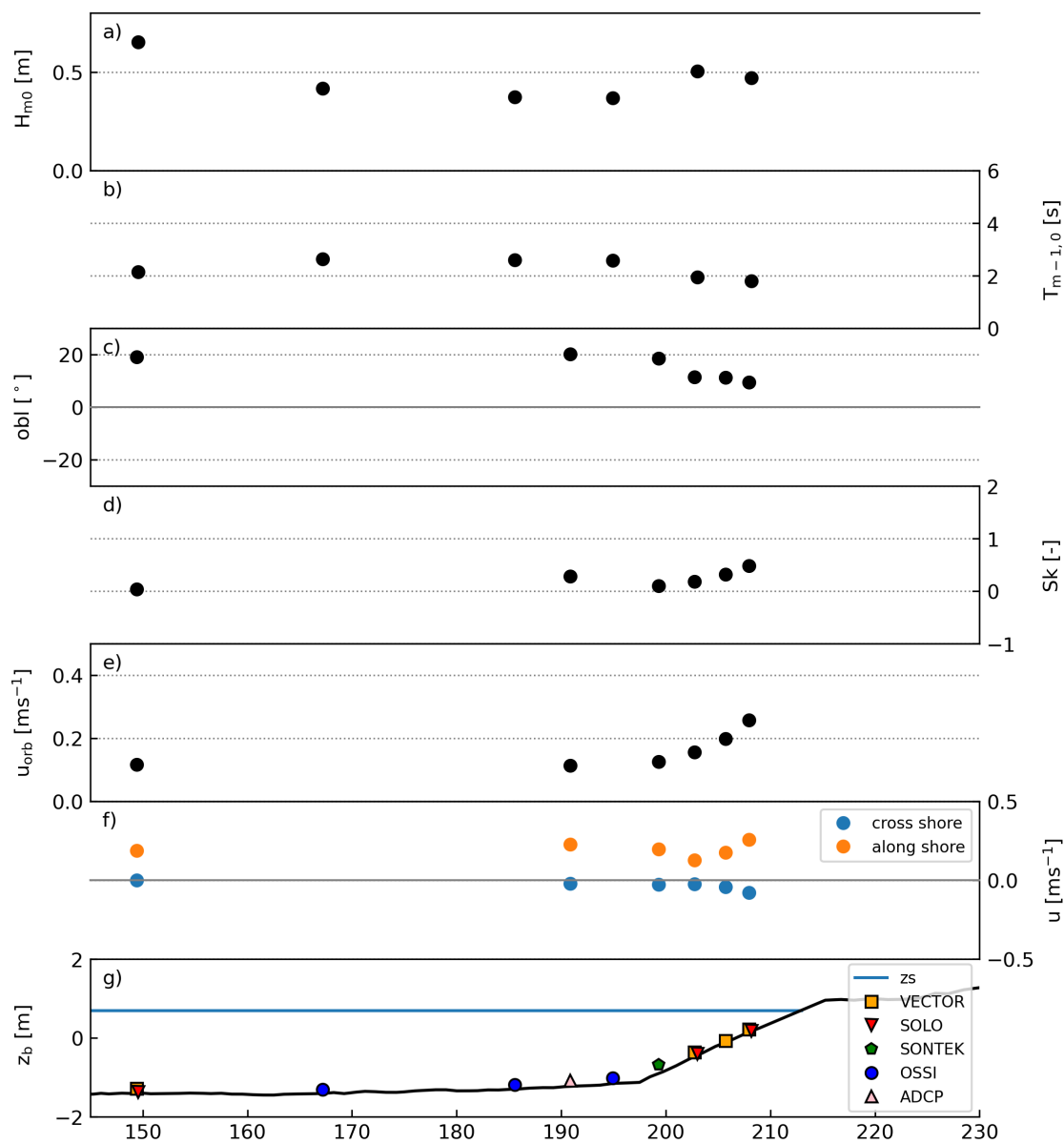


Figure 8. Snapshot of the observed cross-shore wave and current transformation along the cross-shore transect on September-19 08:30: a) significant wave height H_{m0} , b) mean wave period $T_{m-1,0}$, c) wave angle of incidence, d) near-bed velocity skewness, e) near-bed orbital velocity, f) burst mean currents in the cross-shore and alongshore direction, g) position of instruments on the profile with the burst mean water level for reference.

dynamic data and profile development have been published in netCDF format and sediment statistics are published in CSV

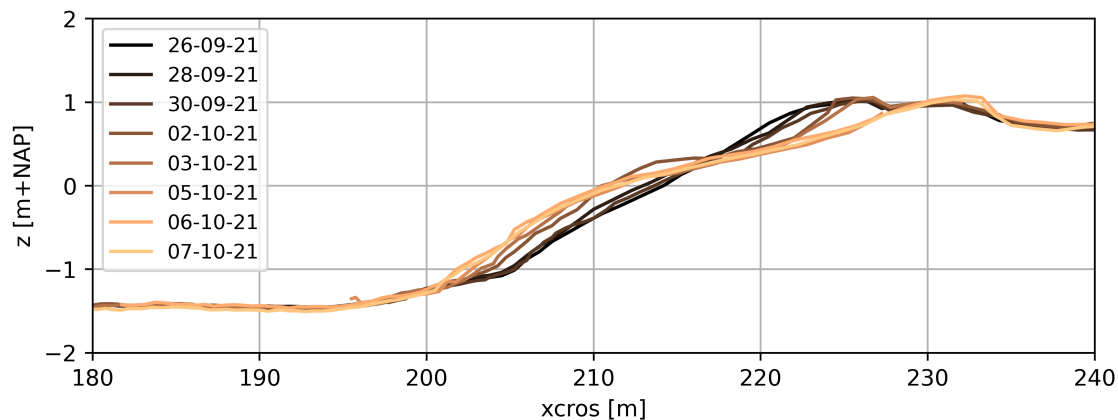


Figure 9. Cross-shore profiles of the Prins Hendrik Zanddijk, measured before and after October-01 on the cross-shore array. See Figure 2 for the transect position.

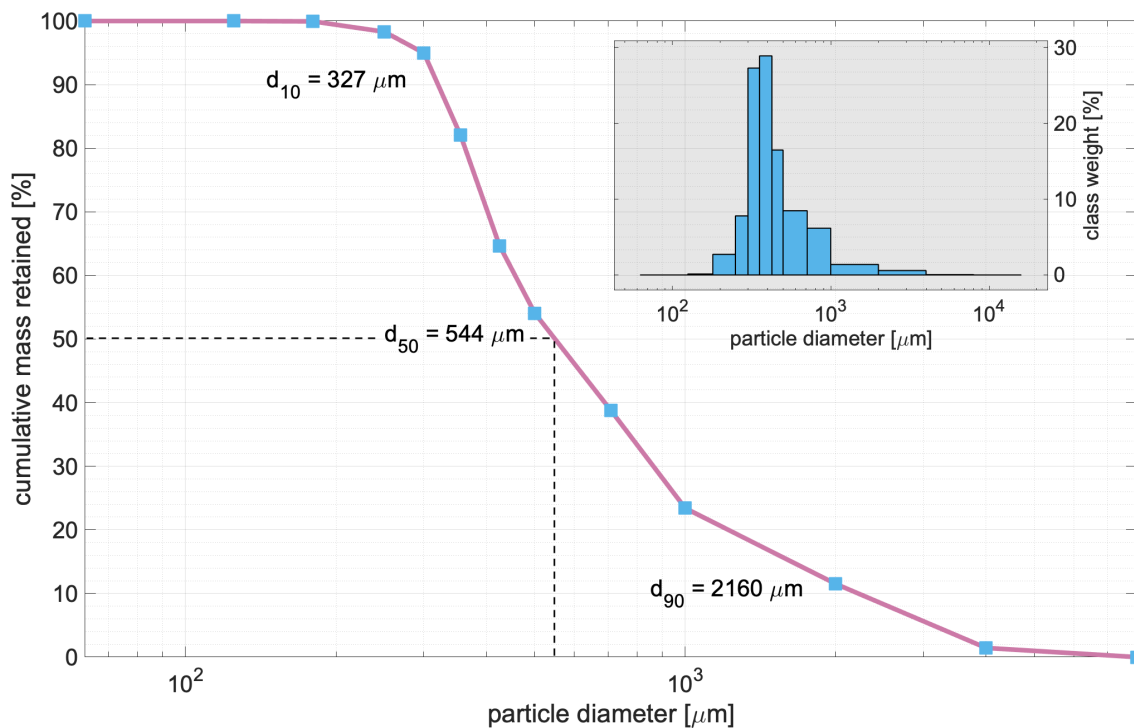


Figure 10. Example of a cumulative grain-size distribution and corresponding bar graph (embedded) of a sediment sample taken around $NAP + 0$ m at alongshore location L2. Black dashed lines indicate the median grain size of the sample.

format. The underlying raw data as produced by the instruments together with the (matlab and python) scripts for conversion
 320 to netCDF with metadata are maintained under version control and are available upon request from the authors.



Sample availability. Remaining dried sample materials are stored in dry storage at the Earth Simulation Laboratory, Princetonlaan 4, 3584 CB Utrecht, the Netherlands. All sample bags are labeled and in most cases contain less than 100 g of sediment, depending on the sample location on the beach (i.e., wetter generally means less sample). These quantities are generally too small for another mechanical-sieving procedure but can still be used for other analysis techniques which require much less material, for instance using a settling tube. Access to
325 the sample collection is possible on request; please contact J.W. Bosma (j.w.bosma@uu.nl).

Author contributions. MvdL: Methodology, Field work, Data Curation and Formal analysis hydrodynamics and beach profiles, Writing – original draft preparation, review and editing. JB: Methodology, Field work, Data Curation and Formal analysis sediment samples and turbidity, Writing – review and editing. MdS: Conceptualization, Supervision, Writing – review and editing. TP: Conceptualization, Supervision, Writing – review and editing. MvM: Methodology, Field work. PvdG: Field work. GR: Conceptualization, Methodology, Supervision. AR:
330 Methodology, Supervision, Writing – review and editing. SA: Conceptualization, Writing – review and editing.

Competing interests. All authors declare they have no competing interests.

Acknowledgements. This work is part of the research program: EURECCA 'Effective Upgrades and REtrofits for Coastal Climate Adaptation' under project number 18035, financed by NWO Domain Applied and Engineering Sciences and supported by Jan De Nul Group, Hoogheemraadschap Hollands Noorderkwartier, Waterproof B.V., Arcadis and Deltares. We thank dredging company Jan De Nul Group in
335 particular for supplying the bathymetric data and deploying the wave buoy in the channel. We would like to thank the staff of the Utrecht University Earth Simulation Lab, in particular Mark Eijkelboom, Henk Markies and Arjan van Eijk, and the staff of the TU Delft Fieldwork Lab, Chantal Willems, Arie van der Vlies and Arno Doorn for all efforts in preparation and execution of this campaign. Special thanks to the dedication of MSc students involved in the campaign: Jelle Woerdman, Martijn klein Obbink, Roel Hoegen, Ruurd Jaarsma and Menno van Maanen.



340 References

- Bergillos, R. J., López-Ruiz, A., Medina-López, E., Moñino, A., and Ortega-Sánchez, M.: The Role of Wave Energy Converter Farms on Coastal Protection in Eroding Deltas, Guadalfeo, Southern Spain, *Journal of Cleaner Production*, 171, 356–367, <https://doi.org/10.1016/j.jclepro.2017.10.018>, 2018.
- Bernabeu, A., Medina, R., and Vidal, C.: A Morphological Model of the Beach Profile Integrating Wave and Tidal Influences, *Marine Geology*, 197, 95–116, [https://doi.org/10.1016/S0025-3227\(03\)00087-2](https://doi.org/10.1016/S0025-3227(03)00087-2), 2003.
- 345 Blott, S. J. and Pye, K.: GRADISTAT: A Grain Size Distribution and Statistics Package for the Analysis of Unconsolidated Sediments, *Earth Surface Processes and Landforms*, 26, 1237–1248, <https://doi.org/10.1002/esp.261>, 2001.
- Brand, E., Ramaekers, G., and Lodder, Q.: Dutch Experience with Sand Nourishments for Dynamic Coastline Conservation – An Operational Overview, *Ocean & Coastal Management*, 217, 106 008, <https://doi.org/10.1016/j.ocecoaman.2021.106008>, 2022.
- 350 Choule J. Sonu: Bimodal Composition and Cyclic Characteristics of Beach Sediment in Continuously Changing Profiles, *SEPM Journal of Sedimentary Research*, Vol. 42, <https://doi.org/10.1306/74D72653-2B21-11D7-8648000102C1865D>, 1972.
- Colosimo, I., Van Maren, D. S., De Vet, P. L. M., Winterwerp, J. C., and Van Prooijen, B. C.: Winds of Opportunity: The Effects of Wind on Intertidal Flat Accretion, *Geomorphology*, p. 108840, <https://doi.org/10.1016/j.geomorph.2023.108840>, 2023.
- Cooper, J. A. G., Pilkey, O. H., and Lewis, D. A.: Islands behind Islands: An Unappreciated Coastal Landform Category, *Journal of Coastal Research*, 2007.
- 355 de Schipper, M. A., de Vries, S., Ruessink, G., de Zeeuw, R. C., Rutten, J., van Gelder-Maas, C., and Stive, M. J.: Initial Spreading of a Mega Feeder Nourishment: Observations of the Sand Engine Pilot Project, *Coastal Engineering*, 111, 23–38, <https://doi.org/10.1016/j.coastaleng.2015.10.011>, 2016.
- Donelan, M., Hamilton, J., and Hui, W.: Directional Spectra of Wind Generated Waves, *Directional spectra of wind-generated ocean waves.*" *Philosophical Transactions of the Royal Society of London. Series A, Mathematical and Physical Sciences*, 315, 509–562, 1985.
- 360 Elgar, S., Raubenheimer, B., and Guza, R. T.: Quality Control of Acoustic Doppler Velocimeter Data in the Surfzone, *Measurement Science and Technology*, 16, 1889–1893, <https://doi.org/10.1088/0957-0233/16/10/002>, 2005.
- Eliot, M. J., Travers, A., and Eliot, I.: Morphology of a Low-Energy Beach, Como Beach, Western Australia, *Journal of Coastal Research*, 221, 63–77, <https://doi.org/10.2112/05A-0006.1>, 2006.
- 365 Ewans, K. C.: Observations of the Directional Spectrum of Fetch-Limited Waves, *Journal of Physical Oceanography*, 28, 495–512, [https://doi.org/10.1175/1520-0485\(1998\)028<0495:OOTDSO>2.0.CO;2](https://doi.org/10.1175/1520-0485(1998)028<0495:OOTDSO>2.0.CO;2), 1998.
- Feddersen, F.: Effect of Wave Directional Spread on the Radiation Stress: Comparing Theory and Observations, *Coastal Engineering*, 51, 473–481, <https://doi.org/10.1016/j.coastaleng.2004.05.008>, 2004.
- Folk, R. L. and Ward, W. C.: Brazos River Bar [Texas]; a Study in the Significance of Grain Size Parameters, *Journal of Sedimentary Research*, 27, 3–26, <https://doi.org/10.1306/74D70646-2B21-11D7-8648000102C1865D>, 1957.
- 370 Freire, P., Ferreira, O., Taborda, R., Oliveira, F., Carrasco, A., Silva, A., Vargas, C., Capitao, R., Fortes, C., Coli, A., and Santon, J.: Morphodynamics of Fetch-Limited Beaches in Contrasting Environments, *Journal of Coastal Research*, SI 56, 183–187, 2009.
- Grunnet, N. M., Ruessink, B., and Walstra, D.-J. R.: The Influence of Tides, Wind and Waves on the Redistribution of Nourished Sediment at Terschelling, The Netherlands, *Coastal Engineering*, 52, 617–631, <https://doi.org/10.1016/j.coastaleng.2005.04.001>, 2005.
- 375 Guillén, J. and Hoekstra, P.: The “Equilibrium” Distribution of Grain Size Fractions and Its Implications for Cross-Shore Sediment Transport: A Conceptual Model, *Marine Geology*, 135, 15–33, [https://doi.org/10.1016/S0025-3227\(96\)00051-5](https://doi.org/10.1016/S0025-3227(96)00051-5), 1996.



- Hallermeier, R. J.: A Profile Zonation for Seasonal Sand Beaches from Wave Climate, *Coastal Engineering*, 4, 253–277, [https://doi.org/10.1016/0378-3839\(80\)90022-8](https://doi.org/10.1016/0378-3839(80)90022-8), 1980.
- Hegermiller, C. A., Warner, J. C., Olabarrieta, M., Sherwood, C. R., and Kalra, T. S.: Modeling of Barrier Breaching During Hurricanes Sandy and Matthew, *Journal of Geophysical Research: Earth Surface*, 127, <https://doi.org/10.1029/2021JF006307>, 2022.
- Hegge, B., A., Eliot, M. J., and Hsu, J.: Sheltered Sandy Beaches of Southwestern Australia, *Journal of Coastal Research*, 12, 748–760, 1996.
- Héquette, A., Hemdane, Y., and Anthony, E. J.: Sediment Transport under Wave and Current Combined Flows on a Tide-Dominated Shoreface, Northern Coast of France, *Marine Geology*, 249, 226–242, <https://doi.org/10.1016/j.margeo.2007.12.003>, 2008.
- Hoefel, F. and Elgar, S.: Wave-Induced Sediment Transport and Sandbar Migration, *Science*, 299, 1885–1887, <https://doi.org/10.1126/science.1081448>, 2003.
- Hopkins, J., Elgar, S., and Raubenheimer, B.: Observations and Model Simulations of Wave-current Interaction on the Inner Shelf, *Journal of Geophysical Research: Oceans*, 121, 198–208, <https://doi.org/10.1002/2015JC010788>, 2016.
- Hopkins, J., Elgar, S., and Raubenheimer, B.: Flow Separation Effects on Shoreline Sediment Transport, *Coastal Engineering*, 125, 23–27, <https://doi.org/10.1016/j.coastaleng.2017.04.007>, 2017.
- Huisman, B., De Schipper, M., and Ruessink, B.: Sediment Sorting at the Sand Motor at Storm and Annual Time Scales, *Marine Geology*, 381, 209–226, <https://doi.org/10.1016/j.margeo.2016.09.005>, 2016.
- Huisman, B., Walstra, D.-J., Radermacher, M., de Schipper, M., and Ruessink, G.: Observations and Modelling of Shoreface Nourishment Behaviour, *Journal of Marine Science and Engineering*, 7, 59, <https://doi.org/10.3390/jmse7030059>, 2019.
- Jackson, N. L. and Nordstrom, K. F.: Site Specific Controls on Wind and Wave Processes and Beach Mobility on Estuarine Beaches in New Jersey, U.S.A., *Journal of Coastal Research*, 8, 88–98, 1992.
- Jackson, N. L., Nordstrom, K. F., Eliot, I., and Masselink, G.: ‘Low Energy’ Sandy Beaches in Marine and Estuarine Environments: A Review, *Geomorphology*, 48, 147–162, [https://doi.org/10.1016/S0169-555X\(02\)00179-4](https://doi.org/10.1016/S0169-555X(02)00179-4), 2002.
- Kleinhans, M. G.: Grain-Size Sorting in Grainflows at the Lee Side of Deltas: Grain Flow Size Sorting, *Sedimentology*, 52, 291–311, <https://doi.org/10.1111/j.1365-3091.2005.00698.x>, 2005.
- Kleinhans, M. G. and Grasmeyer, B. T.: Bed Load Transport on the Shoreface by Currents and Waves, *Coastal Engineering*, 53, 983–996, <https://doi.org/10.1016/j.coastaleng.2006.06.009>, 2006.
- Kroon, A., Hoekstra, P., Houwman, K., and Ruessink, G.: Morphological Monitoring of a Shoreface Nourishment Nourtec: Experiment at Terschelling, The Netherlands, in: *Coastal Engineering 1994*, pp. 2222–2236, American Society of Civil Engineers, Kobe, Japan, <https://doi.org/10.1061/9780784400890.162>, 1995.
- Lemke, L. and Miller, J. K.: EOF Analysis of Shoreline and Beach Slope Variability at a Feeder Beach Constructed within a Groin Field at Long Branch, New Jersey, *Coastal Engineering*, 121, 14–25, <https://doi.org/10.1016/j.coastaleng.2016.11.001>, 2017.
- Ludka, B., Guza, R., and O’Reilly, W.: Nourishment Evolution and Impacts at Four Southern California Beaches: A Sand Volume Analysis, *Coastal Engineering*, 136, 96–105, <https://doi.org/10.1016/j.coastaleng.2018.02.003>, 2018.
- Luijendijk, A. P., Ranasinghe, R., de Schipper, M. A., Huisman, B. A., Swinkels, C. M., Walstra, D. J., and Stive, M. J.: The Initial Morphological Response of the Sand Engine: A Process-Based Modelling Study, *Coastal Engineering*, 119, 1–14, <https://doi.org/10.1016/j.coastaleng.2016.09.005>, 2017.
- Lygre, A. and Krogstad, H.: Maximum Entropy Estimation of the Directional Distribution in Ocean Wave Spectra, *Journal of Physical Oceanography*, 16, 2052–2060, 1986.



- Makaske, B. and Augustinus, P. G. E. F.: Morphologic Changes of a Micro-Tidal, Low Wave Energy Beach Face during a Spring-Neap Tide
415 Cycle, Rhône-Delta, France, *Journal of Coastal Research*, 14, 632–645, 1998.
- Masselink, G. and Short, A. D.: The Effect of Tide Range on Beach Morphodynamics and Morphology: A Conceptual Beach Model, *Journal of Coastal Research*, 9, 785–800, 1993.
- Masselink, G., Russell, P., Blenkinsopp, C., and Turner, I.: Swash Zone Sediment Transport, Step Dynamics and Morphological Response on a Gravel Beach, *Marine Geology*, 274, 50–68, <https://doi.org/10.1016/j.margeo.2010.03.005>, 2010.
- 420 McCarron, C. J., Van Landeghem, K. J., Baas, J. H., Amoudry, L. O., and Malarkey, J.: The Hiding-Exposure Effect Revisited: A Method to Calculate the Mobility of Bimodal Sediment Mixtures, *Marine Geology*, 410, 22–31, <https://doi.org/10.1016/j.margeo.2018.12.001>, 2019.
- Nordstrom, K. F. and Jackson, N. L.: Physical Processes and Landforms on Beaches in Short Fetch Environments in Estuaries, Small Lakes and Reservoirs: A Review, *Earth-Science Reviews*, 111, 232–247, <https://doi.org/10.1016/j.earscirev.2011.12.004>, 2012.
- Pearson, S. G., Verney, R., Van Prooijen, B. C., Tran, D., Hendriks, E., Jacquet, M., and Wang, Z. B.: Characterizing the Composition
425 of Sand and Mud Suspensions in Coastal & Estuarine Environments Using Combined Optical and Acoustic Measurements, Preprint, *Oceanography*, <https://doi.org/10.1002/essoar.10506576.1>, 2021.
- Perk, L., van Rijn, L., Koudstaal, K., and Fordeyn, J.: A Rational Method for the Design of Sand Dike/Dune Systems at Sheltered Sites; Wadden Sea Coast of Texel, The Netherlands, *Journal of Marine Science and Engineering*, 7, 324, <https://doi.org/10.3390/jmse7090324>, 2019.
- 430 Pickrill, R.: Beach Changes on Low Energy Lake Shorelines, Lakes Manapouri and Te Anau, New Zealand, *Journal of Coastal Research*, 1, 353–363, 1985.
- Puleo, J. A., Johnson, R. V., Butt, T., Kooney, T. N., and Holland, K. T.: The Effect of Air Bubbles on Optical Backscatter Sensors, *Marine Geology*, 230, 87–97, <https://doi.org/10.1016/j.margeo.2006.04.008>, 2006.
- Richmond, B. M. and Sallenger, A. H.: Cross-Shore Transport of Bimodal Sands, in: *Coastal Engineering 1984*, pp. 1997–2008, American
435 Society of Civil Engineers, Houston, Texas, United States, <https://doi.org/10.1061/9780872624382.135>, 1985.
- Soulsby, R. L.: Coastal Sediment Transport: The COAST3D Project, in: *Coastal Engineering 1998*, pp. 2548–2558, American Society of Civil Engineers, Copenhagen, Denmark, <https://doi.org/10.1061/9780784404119.192>, 1999.
- Splinter, K. D. and Palmsten, M. L.: Modeling Dune Response to an East Coast Low, *Marine Geology*, 329–331, 46–57, <https://doi.org/10.1016/j.margeo.2012.09.005>, 2012.
- 440 Stive, M. J., De Schipper, M. A., Luijendijk, A. P., Aarninkhof, S. G., Van Gelder-Maas, C., Van Thiel De Vries, J. S., De Vries, S., Henriquez, M., Marx, S., and Ranasinghe, R.: A New Alternative to Saving Our Beaches from Sea-Level Rise: The Sand Engine, *Journal of Coastal Research*, 290, 1001–1008, <https://doi.org/10.2112/JCOASTRES-D-13-00070.1>, 2013.
- Strypsteen, G., van Rijn, L., Hoogland, M., Rauwoens, P., Fordeyn, J., Hijma, M., and Lodder, Q.: Reducing Aeolian Sand Transport and Beach Erosion by Using Armour Layer of Coarse Materials, *Coastal Engineering*, 166, 103 871,
445 <https://doi.org/10.1016/j.coastaleng.2021.103871>, 2021.
- Ton, A. M.: Sandy Beaches in Low-Energy, Ph.D. thesis, Delft University of Technology, Delft, 2023.
- Ton, A. M., Vuik, V., and Aarninkhof, S. G.: Sandy Beaches in Low-Energy, Non-Tidal Environments: Linking Morphological Development to Hydrodynamic Forcing, *Geomorphology*, 374, 107 522, <https://doi.org/10.1016/j.geomorph.2020.107522>, 2021.
- Travers, A.: Low-Energy Beach Morphology with Respect to Physical Setting: A Case Study from Cockburn Sound, Southwestern Australia,
450 *Journal of Coastal Research*, 232, 429–444, <https://doi.org/10.2112/04-0275.1>, 2007.



- Travers, A., Eliot, M. J., Eliot, I. G., and Jendrzczak, M.: Sheltered Sandy Beaches of Southwestern Australia, Geological Society, London, Special Publications, 346, 23–42, <https://doi.org/10.1144/SP346.3>, 2010.
- Valiente, N. G., Masselink, G., Scott, T., Conley, D., and McCarroll, R. J.: Role of Waves and Tides on Depth of Closure and Potential for Headland Bypassing, *Marine Geology*, 407, 60–75, <https://doi.org/10.1016/j.margeo.2018.10.009>, 2019.
- 455 van der Lugt, Marlies.A., Bosma, J. W., De Schipper, M. A., Price, T. D., van Maarseveen, M. C., van der Gaag, P., Reniers, A. J. H. M., Ruessink, B. G., and Aarninkhof, S. G.: SEDMEX: Measurements of Morphodynamics of a Sheltered Beach along the Dutch Wadden Sea, <https://doi.org/10.4121/19c5676c-9cea-49d0-b7a3-7c627e436541.v1>, 2023.
- Van IJendoorn, C. O., Hallin, C., Cohn, N., Reniers, A. J. H. M., and De Vries, S.: Novel Sediment Sampling Method Provides New Insights into Vertical Grain Size Variability Due to Marine and Aeolian Beach Processes, *Earth Surface Processes and Landforms*, 48, 782–800, <https://doi.org/10.1002/esp.5518>, 2023.
- 460 Van Kouwen, N. C., Ton, A. M., Vos, S. E., Vijverberg, T., Reniers, A. J., and Aarninkhof, S. G.: Quantifying Spit Growth and Its Hydrodynamic Drivers in Wind-Dominated Lake Environments, *Geomorphology*, 437, 108 799, <https://doi.org/10.1016/j.geomorph.2023.108799>, 2023.
- Vila-Concejo, A., Hughes, M. G., Short, A. D., and Ranasinghe, R.: Estuarine Shoreline Processes in a Dynamic Low-Energy System, *Ocean Dynamics*, 60, 285–298, <https://doi.org/10.1007/s10236-010-0273-7>, 2010.
- 465 Wilkinson, M. D., Dumontier, M., Aalbersberg, I. J., Appleton, G., Axton, M., Baak, A., Blomberg, N., Boiten, J.-W., Da Silva Santos, L. B., Bourne, P. E., Bouwman, J., Brookes, A. J., Clark, T., Crosas, M., Dillo, I., Dumon, O., Edmunds, S., Evelo, C. T., Finkers, R., Gonzalez-Beltran, A., Gray, A. J., Groth, P., Goble, C., Grethe, J. S., Heringa, J., 'T Hoen, P. A., Hoof, R., Kuhn, T., Kok, R., Kok, J., Lusher, S. J., Martone, M. E., Mons, A., Packer, A. L., Persson, B., Rocca-Serra, P., Roos, M., Van Schaik, R., Sansone, S.-A., Schultes, E., Sengstag, T., Slater, T., Strawn, G., Swertz, M. A., Thompson, M., Van Der Lei, J., Van Mulligen, E., Velterop, J., Waagmeester, A., Wittenburg, P., Wolstencroft, K., Zhao, J., and Mons, B.: The FAIR Guiding Principles for Scientific Data Management and Stewardship, *Scientific Data*, 3, 160 018, <https://doi.org/10.1038/sdata.2016.18>, 2016.
- 470 Wright, L. D. and Short, A. D.: Morphodynamic Variability of Surf Zones and Beaches: A Synthesis, *Marine Geology*, 56, 98–118, 1984.
- Young, I., Verhagen, L., and Khatri, S.: The Growth of Fetch Limited Waves in Water of Finite Depth. Part 3. Directional Spectra, *Coastal Engineering*, 29, 101–121, [https://doi.org/10.1016/S0378-3839\(96\)00026-9](https://doi.org/10.1016/S0378-3839(96)00026-9), 1996.
- 475